SF2A 2009
M. Heydari-Malayeri, C. Reylé and R. Samadi (eds)

SPITZER AND HST TRANSIT SPECTROPHOTOMETRY OF THE EXOPLANET HD189733B

Désert, J.-M.[1], Sing, D. K.[1], Vidal-Madjar, A.[1], Lecavelier des Etangs, A.[1], Hébrard, G.[1], Ehrenreich, D.[2], Ferlet, R.[1], Parmentier, V.[1] and Henry, G.[3]

Abstract.

Transit observations in the infrared allow the atmospheric content of exoplanets to be determined. Here we present new primary transit observations of the hot-jupiter HD 189733b, obtained in the near and mid-IR with Hubble and Spitzer Space Telescopes. The high-S/N photometric transit light curves allow us to improve the precision of the near infrared planet radius. We are able to derive accurate system parameters, including planet-to-star radius ratios, impact parameter, scale of the system, and central time of the transit from fits to the transit light curves. We compare the results obtained here with transmission spectroscopic models and with results from various other observations of this planet. These new observations show that water vapour bandheads are not detected using transmission photometry observations at either 1.6 μm or 3.6 μm. Our results further support that another species must absorb at these wavelengths, at high altitudes, and could be attributed to Rayleigh scattering by haze. Observations at 4.5 μm can also be interpreted as due to the presence of CO and would lead to a large CO/H2O ratio estimated to be between 1 and 60.

1 Introduction

Two hot-Jupiters in particular, HD 189733b and HD 209458b, currently offer the very best laboratories in which to study exoplanet atmospheres and have formed the prototype hot-Jupiter planets. These two planets have the brightest parent stars among transiting planets and contain large transit depths, making precise transmission studies at high signal-to-noise ratios possible. The first transiting planet discovered, HD209458b, holds the distinction of the first detection of an extrasolar planetary atmosphere (Charbonneau et al. 2002) and escaping atmosphere (Vidal-Madjar et al. 2003, 2004, 2008). The optical transmission spectra of this planet shows evidence for several different layers of Na (Sing et al. 2008a,b) as well as Rayleigh scattering by molecular hydrogen (Lecavelier et al. 2008) and the presence of TiO/VO (Désert et al. 2008). The atmospheric Na signature has also been confirmed by ground based observations (Snellen et al. 2008).

HD189733b (Bouchy et al. 2005) is among the closest known transiting planets with a K V type parent star, giving it one of the largest transit and anti-transit signals known. The *Spitzer Space Telescope* (Werner et al. 2004) has revealed its potential to probe exoplanetary atmospheres through emission and transmission spectra. Spitzer anti-transit measurements have shown efficient heat-redistribution, measuring the planets temperature profile from orbital phase curves (Knutson et al. 2007; Knutson et al.2009) and a definitive detection of atmospheric water from emission spectra (Grillmair et al. 2008) and the likely presence of carbon monoxide (CO; Charbonneau et al. 2008). In primary transit, Pont et al. (2008) used the HST/ACS grism to provide the first transmission spectra from 0.6 to 1.0 μm. This spectrum is seen to be almost featureless likely indicating the presence of high altitude haze, with a λ^{-4} wavelength dependence of the spectra likely due to Rayleigh scattering by sub-micron $MgSiO_3$ molecules (Lecavelier et al. 2008). From the ground, Redfield et al. (2008 detected strong Na absorption in the core of the doublet. In the infrared, Swain et al. (2008) used *Near*

[1] UPMC Univ Paris 06, UMR7095, Institut d'Astrophysique de Paris, F-75014, Paris, France

[2] Laboratoire d'Astrophysique, Observatoire de Grenoble, UJF,CNRS;BP 53, F-38041 GRENOBLE Cedex 9 (France)

[3] Center of Excellence in Information Systems, Tennessee State University,3500 John A. Merritt Blvd., Box 9501, Nashville, TN 37209, USA

Infrared Camera and Multi-Object Spectrometer (NICMOS) aboard *HST* and showed evidence for absorption of atmospheric water and methane using spectroscopic observations between 1.5 and 2.5 μm.

Knutson et al. (2007) obtained the first accurate near infrared (NIR) transit measurements for this planet using the Infrared Array Camera (IRAC; Fazio et al. 2004) aboard *Spitzer* at 8.0 μm. The search for molecular spectroscopic signatures by comparing two photometric bands with *Spitzer* has been attempted by Ehrenreich et al. (2007). This study concluded that uncertainties on the measurements were too large to draw firm conclusions on the detection of water at high altitudes. Yet, using the same data set, but a different analysis (Beaulieu et al. 2008), Tinetti et al. (2007) claimed to detect the presence of atmospheric water vapour from comparison of the absorptions at 3.6 μm and 5.8 μm. We recently performed a consistent and complete study of the stellar mode observations obtained with the four IRAC channels (Désert et al. 2009), with a detailed assessment of systematics. We concluded that there is no excess absorption at 5.8 μm compared to 3.6 μm. Moreover, we found that water absorption alone cannot explain the radius at 3.6 μm. Therefore, other species must be present in the atmosphere of the planet and absorb at this wavelength, such as Rayleigh scattering by haze as found by Pont et al. (2008). We also derived a slightly larger radius at 4.5 μm that cannot be explained by H_2O nor Rayleigh scattering. We interpreted this hint of absorption excess as due to the possible presence of CO molecules (Désert et al. 2009) which could be in agreement with the small emission seen with secondary eclipse measurement at the same wavelength (Charbonneau et al. 2008).

Here, we present a joint analysis of our *Spitzer*/IRAC and HST/NICMOS observations of primary transits of HD 189733b. This work is our ongoing efforts to charaterize the transit spectra of HD 189733b using space-based observatories (Désert et al. 2009a,b; Sing et al. 2009). The data consists of high-cadence time series. The photometric precision achieved allows us to derive accurate measurements of the radius used to probe the planet's atmospheric composition. Our results together with a comparison with previous studies and theoretical predictions are given below.

2 Observations and analysis

2.1 Spitzer transit lightcurves

First observations (visit 1 hereafter) of the system were performed on 2006 October 31 simultaneously at 3.6 and 5.8 μm (channels 1 and 3). The second part of the program was completed on November 23, 2007 using the 4.5 and 8 μm channels (channels 2 and 4) following the same methods (visit 2 hereafter). In both visits, the system was observed using IRAC's stellar mode during 4.5 hours for each visit, upon which 1.8h was spent in planetary transit. A third primary transit (visit 3 hereafter) was obtained on 25 November 2007 at 3.6 μm (Channel 1). In that specific case, the system was observed using IRAC's 32×32 pixel subarray mode during 4.5 hours, upon which 1.8h was spent in planetary transit. The details of the analysis of these three visits can be found in Désert et al. (2009a,b).

We used aperture photometry to extract the transit lightcurves in each channel from the *Spitzer*/IRAC Basic Calibrated Data (BCD) frames. These frames are produced by the standard IRAC calibration pipeline and include corrections for dark current, flat-fielding, detector nonlinearity, and conversion to flux units.

After producing a time series, we iteratively select and trim outliers greater than 4 σ by comparing the photometric measurements to the best fit of a transit light curve model. Doing so, we removed any remaining points affected by transient hot pixels. We discarded frames, which represent 0.1% of the total number of photometric data points.

We finally modeled the transit light curve with 4 parameters: the planet-star radius ratio $R_p/R_\star$, the orbital distance to stellar radius ratio (system scale) $a/R_\star$, the impact parameter b, and the time of mid-transit T_c. We used the IDL transit routine `OCCULTNL` developed by Mandel & Agol (2002) for the transit light curve model. We took into account limb darkening correction using a three non-linear limb-darkening coefficients. We performed a least-squares fit to our transit light curves simultaneously over the whole parameter space ($R_p/R_\star$, $a/R_\star$, b, T_c). We used the Prayer Bead method (Moutou et al. 2004; Gillon et al. 2007) to determine the mean value as well as the statistical and systematical errors for the measured parameters.

Nevertheless, the transit lightcurves are affected by systematical effects that have to be taken into account and properly corrected to determine the correct parameters. The pixel phase effect is predominant at shorter wavelength whereas the ramp effect affected longer wavelength. These effects and their corrections are described below.

2.1.1 Pixel phase effect decorrelation

Because of instrumental effects, the measured stellar flux out-of-transit is not constant, but is seen to vary in time. Telescope jitter and intra-pixel sensitivity variations are responsible for fluctuations seen in the centroid and in the raw light curves. A description of this effect, known as the pixel-phase effect, is given in the *Spitzer*/IRAC data handbook (Reach et al. 2006, p. 50; see also Charbonneau et al. 2005) and affect mainly Channels 1 and 2. To correct for this instrumental effect, we defined a baseline function which is a quadratic function of X and Y target positions, with five parameters K_i, as described in Désert et al. (2009). This function is more robust against systematics compared to a function with one parameter used by the previous analyses (Ehrenreich et al. 2007; Beaulieu et al. 2008).

2.1.2 Baseline

The baselines are known to be inherently linear for channel 1 and 2 and logarithmic for channel 3 and 4 (Knutson et al. 2008). However, we tested three different baselines functions: polynomial of one, two and three degrees, an exponential with a polynomial, and logarithmic with a linear function. We tested the robustness of each of these different baselines by dropping the first exposures from the beginning of the observations (exposure with a phase smaller than -0.03). We found that for channels 3 and 4, the best fits are obtained when using a logarithmic baseline (see lower panel in Fig. 2). In the case of a linear, polynomial or exponential baseline, the fitted parameters show large residuals and large scatter with the number of data point removed. The radius dramatically changes according to the number of points removed when using a linear or a third degree polynomial baseline functions indicating that systematics errors remain in the corrected data. In the case of a logarithmic baseline, the radius extracted does not depend on the number of removed points. The logarithmic function is the only one which allows the observable parameters to oscillate around the same value independently of removed exposures. Only small systematics still remain and they are included in the final error bar.

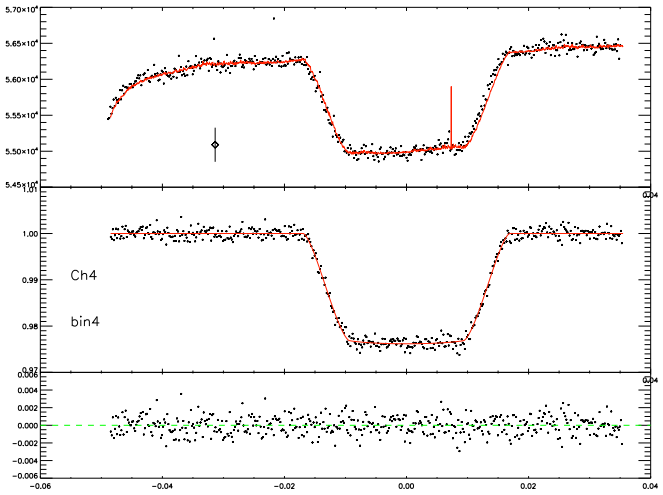

Fig. 1. Channel 4. Top panel: The full raw transit light curve (TLC) with its best fit model (red line). The ramp effect can be easelly seen at the begining of the TLC. Middle panel: Normalized TLC corrected for the ramp and pixel phase effect. Bottom panel: Root-mean-square (RMS) resulting from the best fit model. The fit is always better when using the logarithmic function. This is particularly true at the beginning of the time series, where the ramp effect is the strongest.

2.2 HST transit lightcurves

We observed HD189733 during five transits using the Near Infrared Camera and Multi Object Spectrometer (NICMOS) aboard the Hubble Space Telescope during Cycle 16. Each transit observation consisted of four consecutive spacecraft orbits, each roughly centered on a transit event. For each transit event, we obtained

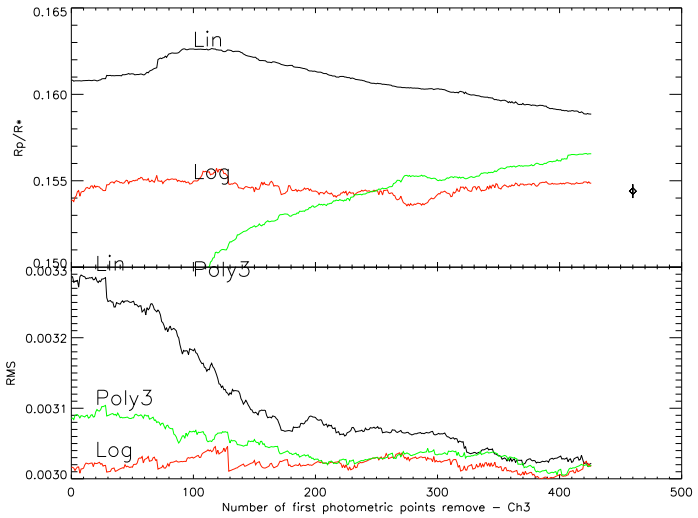

Fig. 2. Channel 3. Top panel: $R_p/R_\star$ ratios extracted when using linear, polynomial of a 3rd degree, and logarithmic baselines as function of the number of first photometric points removed from which the transit light curve is fitted. In the abscisse, 0 point removed correspond to the full transit light curve (TLC). The left over TLC when padded at a phase of -0.03 correspond to the removal of nearly ~ 430 measured points. The diamond point on the right hand side with its error bar, indicates the mean value with its error bar obtained by bootstrap when using a logarithmic baseline. Bottom panel: Root-mean-square (RMS) resulting from the fit using the three different baselines describe above as function of first exposures removed. The fit is always better when using the logarithmic function. This is particularly true at the beginning of the time series, where the ramp effect is the strongest.

images using the high resolution NIC1 camera with only a single narrowband filter, using either the F166N filter centered at 1.6607 μm ($\Delta\lambda = 0.0170\mu$m) or the F187N filter centered at 1.8748 μm ($\Delta\lambda = 0.0191\mu$m).

We performed aperture photometry on the calibrated STScI pipeline reduced images. The pipeline includes corrections for bias subtraction, dark current, detector non-linearities, and applies a flat field calibration. The aperture location for each image was determined using a two dimensional Gaussian fit of the point spread function (PSF) for each image. We found apertures with a radii of 15.2 pixels for the F187N filter and 14.7 pixels for the F166N filter minimized the standard deviation of the out-of-transit light curves. The background in our short exposures was found to be negligible, typically accounting for only $\sim$50 total counts per image.

2.3 Three parameter non-linear limb-darkening law

For solar-type stars at near-infrared and infrared wavelengths, the strength of stellar limb-darkening is weaker compared to optical wavelengths. However, the intensity distribution is increasingly non-linear at these longer wavelengths, which require adopting non-linear limb-darkening laws that we took into account when fitting high S/N transit light curves.

2.4 Monitoring the stellar activity

We monitored the stellar activity of HD189733 using both ground-based data as well as the absolute flux level from the NICMOS instrument itself. The ground-based coverage was provided by the T10 0.8 m Automated Photoelectric Telescope (APT) at Fairborn Observatory in southern Arizona (Henry et al. 2008). The near-IR flux levels for HD189733, during our five visits, are based on the baseline flux level from each transit light-curve as well as the first 50 exposures obtained in the filter opposite to that of the transit (ie. F166N or F187N).

Finally, we followed the same methodology as the one described above for the *Spitzer*lightcurves and both results are presented below.

3 Results

As seen here, IRAC (Désert et al. 2009a,b) and NIMCOS (Sing et al. 2009) photometry can provide robust methods for obtaining precision near and mid-infrared transit radii. With carefully selected band filters, we are able to provide stringent constraints on the presence of H_2O absorption features, finding instead upper-atmospheric haze provides sufficient opacity in slant transit geometry to obscure the near and mid-IR molecular signatures. While absorption due to H_2O were reported by Tinetti et al. (2007) and Swain et al. (2008), our both independant observation with IRAC and NICMOS rule out any such feature at 5σ and find their observed feature is likely artifacts of residual systematic errors in both cases. The planetary radii values from Pont et al. (2008) and this work indicate that Rayleigh scattering dominates the broadband transmission spectrum from at least 0.5-2 μm, with sub-micron $MgSiO_3$ haze particles a probable candidate (Lecavelier et al. 2008). The transition wavelength between the transmission spectra being dominated by haze particles and molecular features would seem to be between 2 and 3 μm, as the IRAC spitzer photometry between 3 and 8 microns all show planet radii in excess of those predicted by Rayleigh scattering (Désert et al. 2009a,b).

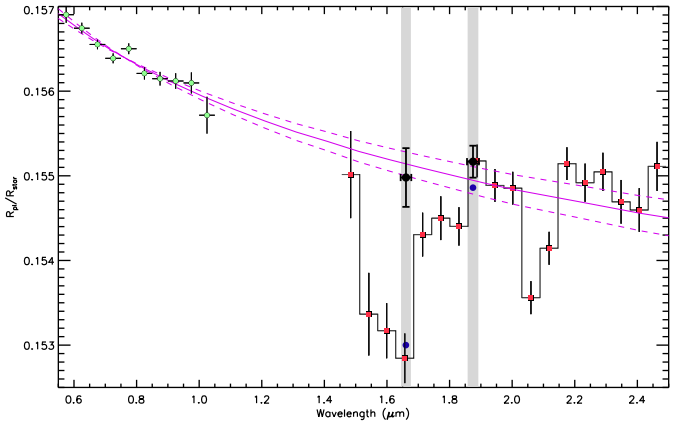

Fig. 3. Measured planetary radii for HD189733b at optical and near-infrared wavelengths. Plotted are the results from our NICMOS narrowband photometry (black dots), along with the NICMOS grism spectrum (red squares) from Swain et al. (2008), and ACS grism spectrum (green dots) from Pont et al. (2008). The 1-σ error bars on the fit radii are indicated (y-axis error bars), along with the wavelength range of each observation (x-axis error bars, grey vertical bars). Also plotted (purple) is the prediction by Rayleigh scattering due to haze from Lecavelier et al. (2008), projected here into the near-infrared along with the 1-σ error on the predicted slope (purple, dashed lines). The NICMOS spectrum from Swain et al. (2008) is quoted as being uncertain in its absolute flux level by $\pm 2\times10^{-4}$ ($\pm$0.00064 $R_{pl}/R_\star$), an offset of -0.00042 $R_{pl}/R_\star$ was applied here for comparison reasons such that the values at 1.87 μm match. Our 1.66μm results are in disagreement with the both the Swain et al. spectra and the expected H_2O atmospheric signature (blue dots), but are in excellent agreement with the predicted planetary radii values from atmospheric haze.

References

Beaulieu, J. P., Carey, S., Ribas, I., & Tinetti, G. 2008, ApJ, 677, 1343
Bouchy, F., et al. 2005, AA, 444, L15
Charbonneau, D., Brown, T. M., Noyes, R. W., & Gilliland, R. L. 2002, ApJ, 568, 377
Charbonneau, D., et al. 2005, ApJ, 626, 523
Charbonneau, D., Knutson, H. A., Barman, T., Allen, et al., & Udry, S. 2008, ApJ, 686, 1341
Désert, J.-M., Vidal-Madjar, A., Lecavelier Des Etangs, A., Sing, et al., R. 2008, AA, 492, 585

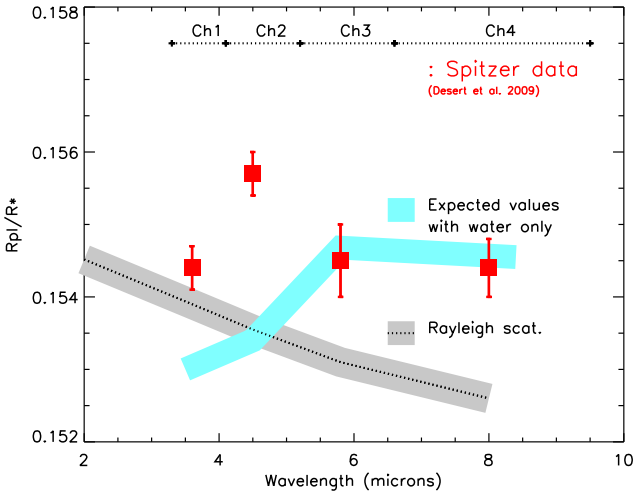

Fig. 4. Census of the measured values of $R_p/R_\star$ ratios in the four *Spitzer*/IRAC channels for HD 189733b obtained from the observations of three transits. Results from our previous analysis of stellar mode observations are plotted with red squares and are shown with their 1 σ errorbars.(Désert et al. 2009). The IRAC bandpasses for each channel are shown with dotted line. The $R_p/R_\star$ ratio obtained at 3.6 μm in subarray mode is 10 σ larger than expected with water absorption only (light blue line) and is consistent with what is expected with Rayleigh scattering by small particles (grey dotted line). The $R_p/R_\star$ obtained at 4.5 μm is larger (4 σ) than expected with either water absorption only or with Rayleigh scattering by small particles. This supplementary absorption could be due to the presence of CO molecules in the planetary atmosphere. The $R_p/R_\star$ obtained at 5.8 μm and at 8.0 μm are consistent with absorption by water vapour.

Désert, J.-M., Lecavelier des Etangs, A., Hébrard, G., Sing, D. K., Ehrenreich, et al., A. 2009, ApJ, 699, 478
Désert, J.-M. et al. submitted
Ehrenreich, D., Hébrard, G., Lecavelier des Etangs, A., Sing, D. K., Désert, J.-M., et al., A. 2007, ApJL, 668, L179
Fazio, G. G., et al. 2004, ApJS, 154, 10
Gillon, M., et al. 2007, AA, 471, L51
Grillmair, C. J., et al. 2008, Nature, 456, 767
Henry, G. W., & Winn, J. N. 2008, AJ, 135, 68
Knutson, H. A., et al. 2009, ApJ, 690, 822
Knutson, H. A., Charbonneau, D., Allen, L. E., Burrows, A., & Megeath, S. T. 2008, ApJ, 673, 526
Knutson, H. A., et al. 2007, Nature, 447, 183
Lecavelier Des Etangs, A., Vidal-Madjar, A., Désert, J.-M., & Sing, D. 2008, AA, 485, 865
Mandel, K., & Agol, E. 2002, ApJL, 580, L171
Moutou, C., Pont, F., Bouchy, F., & Mayor, M. 2004, AA, 424, L31
Pont, F., et al. 2007, AA, 476, 1347
Pont, F., Knutson, H., Gilliland, R. L., Moutou, C., & Charbonneau, D. 2008, MNRAS, 385, 109
Redfield, S., Endl, M., Cochran, W. D., & Koesterke, L. 2008, ApJL, 673, L87
Sing, D. K., Vidal-Madjar, A., Désert, J.-M., Lecavelier des Etangs, A., & Ballester, G. 2008, ApJ, 686, 658
Sing, D. K., Vidal-Madjar, A., Lecavelier des Etangs, A., Désert, J.-M., et al., D. 2008, ApJ, 686, 667
Sing, D. K., Désert, J.-M., Lecavelier Des Etangs, A., Ballester, et al. 2009, AA, 505, 891
Snellen, I. A. G., Albrecht, S., de Mooij, E. J. W., & Le Poole, R. S. 2008, AA, 487, 357
Swain, M. R., Vasisht, G., & Tinetti, G. 2008, Nature, 452, 329
Tinetti, G., et al. 2007, Nature, 448, 169
Vidal-Madjar, A., et al. 2004, ApJL, 604, L69
Vidal-Madjar, A., Lecavelier des Etangs, A., Désert, J.-M., et al. 2008, ApJL, 676, L57
Vidal-Madjar, A., Lecavelier des Etangs, A., Désert, J.-M., Ballester, et al. 2003, Nature, 422, 143
Werner, M. W., et al. 2004, ApJS, 154, 1